Adsorption of Hydrophobin on Different Self-Assembled Mono layers: The Role of the Hydrophobic Dipole and the Electric Dipole

ARTICLE *in* LANGMUIR · SEPTEMBER 2014

Impact Factor: 4.46 · DOI: 10.1021/la502595t · Source: PubMed

4 AUTHORS, INCLUDING:

Jian Zhou
South China University of Technology
84 PUBLICATIONS **1,594** CITATIONS

Langmuir

Article

pubs.acs.org/Langmuir

Adsorption of Hydrophobin on Different Self-Assembled Monolayers: The Role of the Hydrophobic Dipole and the Electric Dipole

Chunwang Peng, Jie Liu, Daohui Zhao, and Jian Zhou*

School of Chemistry and Chemical Engineering, Guangdong Provincial Key Lab for Green Chemical Product Technology, South China University of Technology, Guangzhou, Guangdong 510640, P. R. China

Supporting Information

ABSTRACT: In this work, the adsorptions of hydrophobin (HFBI) on four different self-assembled monolayers (SAMs) (i.e., CH_3-SAM, OH-SAM, COOH-SAM, and NH_2-SAM) were investigated by parallel tempering Monte Carlo and molecular dynamics simulations. Simulation results indicate that the orientation of HFBI adsorbed on neutral surfaces is dominated by a hydrophobic dipole. HFBI adsorbs on the hydrophobic CH_3-SAM through its hydrophobic patch and adopts a nearly vertical hydrophobic dipole relative to the surface, while it is nearly horizontal when adsorbed on the hydrophilic OH-SAM. For charged SAM surfaces, HFBI adopts a nearly vertical electric dipole relative to the surface. HFBI has the narrowest orientation distribution on the CH_3-SAM, and thus can form an ordered monolayer and reverse the wettability of the surface. For HFBI adsorption on charged SAMs, the adsorption strength weakens as the surface charge density increases. Compared with those on other SAMs, a larger area of the hydrophobic patch is exposed to the solution when HFBI adsorbs on the NH_2-SAM. This leads to an increase of the hydrophobicity of the surface, which is consistent with the experimental results. The binding of HFBI to the CH_3-SAM is mainly through hydrophobic interactions, while it is mediated through a hydration water layer near the surface for the OH-SAM. For the charged SAM surfaces, the adsorption is mainly induced by electrostatic interactions between the charged surfaces and the oppositely charged residues. The effect of a hydrophobic dipole on protein adsorption onto hydrophobic surfaces is similar to that of an electric dipole for charged surfaces. Therefore, the hydrophobic dipole may be applied to predict the probable orientations of protein adsorbed on hydrophobic surfaces.

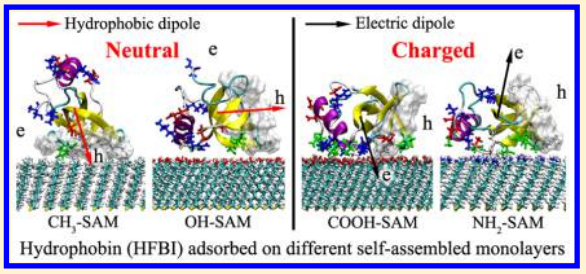

Hydrophobin (HFBI) adsorbed on different self-assembled monolayers

1. INTRODUCTION

The interaction of proteins with material surfaces is of great importance in a broad range of applications in biotechnology and biomolecular engineering.[1] The key issue in all of these applications is the bioactive state of the protein, which is primarily determined by its orientation and conformation. The control of protein orientation on surfaces is critical to retaining and maximizing protein functionality for their applications. For protein adsorption, driving forces and factors regulating protein orientation differ for surfaces with different chemistry. It has been recognized that the orientation of a protein adsorbed on a charged surface is dominated by its electric dipole.[2−8] Due to the charge distribution in a protein, its orientation can be controlled by the polarity of electrostatic charges of the surface. For the adsorption of a protein with a large electric dipole on a strongly charged surface, the direction of the electric dipole is inclined to be almost perpendicular to the surface. Moreover, with the increase of the surface charge density (SCD), the direction of the electric dipole tends to be more vertical and its magnitude also increases.[6] When dominated by electrostatic interactions, the adsorption is highly affected by solution conditions, such as pH and ionic strength (IS). The roles of pH and IS played in protein adsorption have been studied by both experiments[9−12] and simulations.[5,13] The electrostatic interactions between a protein and a charged surface can be screened by a high IS.[4,5] A counterion layer might be formed near the surface when the SCD and IS are high.[13] The protonation of both a protein and a surface will be affected by solution pH. Generally, the maximum adsorption can be obtained near the isoelectric point. However, factors that control the orientation of a protein on a neutral surface remain unresolved.

Hydrophobic moment is a concept first introduced by Einsenberg et al.[14] in 1982; it was used to analyze the amphiphilicity of a protein segment. The zeroth-order hydrophobic moment, or zeroth moment, is defined as the sum of the hydrophobicities of the amino acid residues in a protein; it is analogous to the net charge of a cluster of point charges. The first-order hydrophobic moment, or hydrophobic dipole moment, is similar to the electric dipole moment of a cluster of charges. Just as the electric dipole measures the asymmetry of the charge distribution, the hydrophobic dipole measures the

Received: July 2, 2014
Revised: August 28, 2014
Published: September 3, 2014

amphiphilicity (asymmetry of hydrophobicity) of a complicated molecule. The second-order hydrophobic moment, or quadrupole moment, akin to the electrostatic quadrupole, is used to describe the hydrophobic distribution of a protein.[14] The hydrophobic moment plot[15−18] has been used to identify α-helices involved in the interactions of membrane proteins with lipid bilayers. It has also been used to measure the amphiphilicity of primary and secondary structures either in globular proteins[14,19,20] or in transmembrane proteins.[15,18] It can be useful in many applications, such as relating the function and secondary structure of a protein fragment to its amino-acid sequence, serving as a simple and pictorial summary of some of the forces at work in the folding of proteins,[14] and assisting in identifying regions of functional interest.[20] However, how the hydrophobic dipole affects protein adsorption onto hydrophobic surfaces is still to be addressed.

The hydrophobic effect, i.e., the poor solvation of nonpolar parts of molecules, plays a key role in protein folding and more generally for molecular self-assembly and aggregation in aqueous media or adsorption on solid surfaces.[21] It is believed that, when the surface is hydrophobic, adsorption of any type of protein is very likely because dehydration of that surface easily outweighs electrostatic interactions.[22] This often leads to a relatively large conformation change of the protein.[13] For a neutral hydrophilic surface, however, the protein adsorption is always weak and/or reversible.[23−25] When the surface is zwitterionic, it exhibits high resistance to protein adsorption due to the strong repulsive force exerted by the tightly bound hydration water layer adjacent to the surface.[13,25,26]

Hydrophobins are small fungal proteins, which are highly surface active and possess a unique ability to form amphiphilic membranes through spontaneous self-assembly.[27,28] They are small proteins (7−15 kDa) with a hydrophobic patch at one side and a hydrophilic α-helix at the other side, which have been the object of increasing interest for surface modification owing to their intrinsic biocompatibility and remarkable structural features.[29] They have potentials for numerous applications, such as antifouling, surface coating of biomaterials, modification of electrodes, beer gushing, stabilizing emulsions, separation technologies, etc.[28,30,31] On the basis of the amino acid sequence, hydrophobins are divided into two classes. Class I generally forms highly insoluble films, whereas the films formed by class II have been found to be more soluble. The most studied hydrophobins are the SC3 (class I) from *Schizophyllum commune* and the HFBI and HFBII (class II) from *Trichoderma reesei*.[32]

The adhesion of hydrophobins to hydrophobic surfaces (e.g., polydimethylsiloxane (PDMS), silicon, carbon nanotube, graphite, and polystyrene) and assembly at the air/oil−water interface have been studied.[27,28,30,31] Simulations of hydrophobin adsorption on hydrophobic surfaces (such as PDMS,[33] silicon,[34] graphite,[35] single-walled carbon nanotubes,[36] and methyl-terminated films[37]) and assembly at the air/oil−water interface[38,39] have also been reported. Experimentally, it is already known that hydrophobin can self-assemble into a monolayer on hydrophobic surfaces with its hydrophobic patch binding to the surface and exposing its hydrophilic side outward, thus reversing the inherent hydrophobicity of the surface. However, the mechanisms for the assembly of hydrophobins on hydrophilic surfaces have not yet been fully understood.[12] There are already some studies about the adsorption of hydrophobins on hydrophilic or charged surfaces, such as glass,[27] mica,[27] charged self-assembled monolayers (SAMs),[12] and silicon oxynitride.[32] Experimental results have shown that the highest water contact angle (WCA) could be obtained on cationic surfaces and the binding to these surfaces depended on both pH and IS.[12] However, the mechanisms for these bindings remain to be further studied.

Molecular dynamics (MD) simulations are well-suited to the study of orientation and conformation change of proteins/peptides adsorbed on solid surfaces and could provide molecular level details.[6,7,22−25,40−46] In this work, the adsorption of a class II hydrophobin (HFBI) on four different types of SAM surfaces will be investigated through a combined parallel tempering Monte Carlo (PTMC) and all-atom MD simulation approach. These SAMs are terminated with the methyl ($-CH_3$), hydroxyl ($-OH$), carboxyl ($-COOH$), and amino ($-NH_2$) groups and represent hydrophobic, hydrophilic, negatively charged, and positively charged surfaces, respectively. The orientation and conformation of HFBI on these surfaces will be analyzed. The different roles that the hydrophobic dipole and the electric dipole play in controlling the orientation of HFBI on different surfaces will be discussed. The driving forces for protein adsorption on these surfaces will be revealed. The interfacial water behaviors between the protein and the surfaces will also be studied.

2. MATERIALS AND METHODS

2.1. Hydrophobic Dipole. If the three-dimensional structure of a protein is known, the hydrophobic dipole of the protein can be calculated by $\mathbf{H}_m = \sum_{i=1}^{N} H_i \mathbf{s}_i$, in which H_i is the numerical hydrophobicity of the ith residue, N is the total number of residues, and $\mathbf{s}_i$ is a unit vector pointing from the α-carbon atom of the ith residue to the center of the residue's side chain.[14] A large hydrophobic dipole moment (H_m) indicates the structure is predominantly hydrophobic on one side and predominantly hydrophilic on the other side.

Several hydrophobicity scales[14,15,47] have been published for various uses. The scale used in this work is the normalized "consensus" scale,[15] as it has been used to study the interactions between membrane proteins and lipid bilayers,[15−18] which is quite similar to the protein−SAM system in this work. These values are shown in Table 1. We have also tried the commonly used Kyte−Doolittle scale[47] and the "consensus" scale.[14] The orientations of the hydrophobic dipole calculated from these scales are almost the same with a variation of the magnitudes. The normalized "consensus" scale gets a medium value.

Table 1. Normalized "Consensus" Hydrophobicity Scale[15] Used in This Study

residue	H_m	residue	H_m
Ile	1.38	Pro	0.12
Phe	1.19	Thr	−0.05
Val	1.08	Ser	−0.18
Leu	1.06	His	−0.40
Trp	0.81	Glu	−0.74
Met	0.64	Asn	−0.78
Ala	0.62	Gln	−0.85
Gly	0.48	Asp	−0.90
Cys	0.29	Lys	−1.50
Tyr	0.26	Arg	−2.53

2.2. Protein and Surfaces. *HFBI.* The initial coordinates of HFBI were taken from the tetrameric crystal structure[29] available in the protein data bank (PDB code: 2FZ6). It has been shown that HFBI exists primarily as monomers at low concentrations[48,49] and there is not a strong relationship between HFBI solution association state and surface properties such as surface activity.[50] Therefore, in this work,

dx.doi.org/10.1021/la502595t | *Langmuir* 2014, 30, 11401−11411

only the monomer form is considered for further investigation. The three missing residues, that is, Ser1, Gly74, and Ala75, were repaired by using the program Swiss-Pdb Viewer.[51] Hydrogen atoms were added by the GROMACS 4.5.4 package.[52] The protein was simulated at a neutral pH. The arginine and lysine residues along with the N-terminal were taken to be protonated, whereas the aspartic acid residues and the C-terminal were taken to be deprotonated. The protein has a total of 1030 atoms with a net charge of 0. There are four negatively charged residues (Ser1, Lys32, Arg45, and Lys50) and four positively charged residues (Asp30, Asp40, Asp43, and Ala75), which makes the protein bear an electric dipole moment of about 104 D. From another point of view, as shown in Figure 1, one end of HFBI is

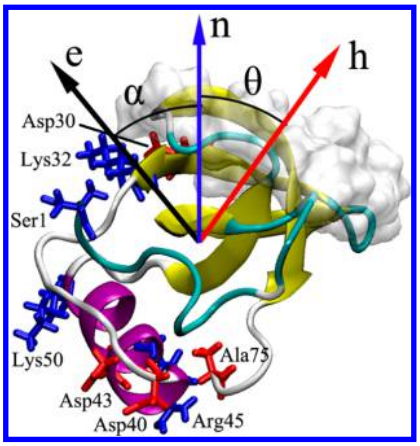

Figure 1. Illustration of orientation angles within HFBI. The blue arrow (**n**), the black arrow (**e**) and the red arrow (**h**) represent the directions of the surface normal, electric dipole, and hydrophobic dipole, respectively. The protein is represented in NewCartoon mode; the white and transparent area represents the hydrophobic patch. Charged amino acids are represented in Licorice mode, with the positively charged residues colored in blue and the negatively charged residues colored in red.

the hydrophobic patch (Leu12, Val23, Leu24, Leu26, Ile27, Leu29, Val59, Ala60, Val62, Ala63, Ala66, Leu67, and Leu68)[29] and the other end is the hydrophilic α-helix (residues 40−50), which endows HFBI a hydrophobic dipole moment of 16.1 nm. The potential parameters for HFBI are from the CHARMM27 force field.[53]

SAMs. The $(\sqrt{3} \times \sqrt{3})$R30° lattice structure[24] was adopted for SAMs of $S(CH_2)_{10}CH_3$, $S(CH_2)_{11}OH$, $S(CH_2)_{10}COOH$, and $S(CH_2)_{11}NH_2$ in all-atom MD simulations. The surface consists of 132 thiol chains with dimensions of 5.494 nm × 5.191 nm. For the COOH-SAM and NH_2-SAM, 10 (about 7.5% dissociation degree) and 20 (about 15% dissociation degree) chains are deprotonated or protonated, representing a SCD of 0.05 and 0.1 C/m^2, respectively. All sulfur atoms in the SAMs were kept fixed during simulations. The potential parameters for SAMs are also from the CHARMM27 force field.[53]

2.3. PTMC Simulations. For the united-residue model of a protein, each amino acid is reduced to a sphere centered at its α-carbon, in which the basic structure information on the protein is well kept.[4] The charged surface is treated to be flat. There are both electrostatic and van der Waals (vdW) interactions between the surface and the protein. The parameters were taken from our previous works.[4,5,7] During PTMC simulations, the protein was kept rigid. N replicas were simulated in parallel, each in the canonical ensemble and at a different temperature T. The details are the same as interpreted in our previous works.[4,5,7] The MC simulation in each replica was carried out in a box of 10 × 10 × 10 nm^3. The protein was initially put in the center of the simulation box. Then, with translational and rotational moves around its center of mass, 40 000 000 MC cycles were carried out with the former 20 000 000 for equilibrium and the latter 20 000 000 for production. The displacement of each move was adjusted to ensure an acceptance ratio of 0.5. Six replicas, with temperatures of 300, 350, 450, 550, 650, and 750 K, respectively, have been used to ensure sufficient energy overlap between neighboring replicas to allow for the acceptance of configuration swaps in each system. The swaps are performed every 500 cycles. The preferential orientations for each system were taken as the initial configurations for further MD simulations.

2.4. MD Simulations. The preferential orientations from PTMC simulations were chosen as the starting points for the following MD simulations. About 5700 water molecules described by the TIP3P model[54] were added to the simulated boxes. Chlorine and sodium ions were added to keep the system neutral with a concentration of 0.01 M. The dimension of the systems is 5.494 × 5.191 × 8 nm^3, and there are about 23 000 atoms in each system. The initial velocity of each atom was assigned from a Maxwell−Boltzmann distribution at 300 K. The simulations were performed in a canonical ensemble with a time step of 2 fs, and the temperature was controlled at 300 K by a Nosé−Hoover thermostat[55] using a coupling time of 0.5 ps. Bonds containing hydrogen were constrained by the LINCS algorithm.[56] The non-bonded interactions were calculated by a switched potential with a switch function starting at 9 Å and reaching zero at 10 Å. Electrostatic interactions were calculated by the particle mesh Ewald (PME) method in 3dc geometry[57] with a cutoff distance of 11 Å. Periodic boundary conditions were applied only in the x and y directions. Two hard walls were set at both the top and the bottom of the simulation box as implemented in the GROMACS 4.5.4 package.[52] The systems were first minimized using the steepest descent method to eliminate the steric overlap or inappropriate geometry. Then, a 100 ps NVT equilibration with a position restraint on heavy atoms of the protein was conducted for each system to equilibrate the solvent and ions around the protein. Finally, an 80 ns MD simulation was performed for each system. For structure visualization, the Visual Molecular Dynamics (VMD) program[58] was used.

2.5. Orientation Characterization. The orientation angle is used to quantitatively characterize the protein orientation on surfaces. For the hydrophobic orientation angle (θ), it is defined as the angle between the surface normal (**n**) and the direction of the hydrophobic dipole (**h**) (as shown in Figure 1). For an angle of 0°, the dipole is parallel to the surface normal; for 90°, it is parallel to the surface; for 180°, it is antiparallel to the surface normal. The electric dipole (**e**)[4,5,7] (as shown in Figure 1) is defined as $\boldsymbol{\mu} = \sum_{i=1}^{N} q_i(\mathbf{r}_i - \mathbf{r}_{COM})$, where q_i is the partial charge of atom i and $\mathbf{r}_i$ and $\mathbf{r}_{COM}$ are the position of atom i and the center of mass of the protein, respectively. The electric orientation angle (α)[7] for the electric dipole is defined in a similar way. Another orientation angle (defined as the "helix-patch")[33] between the vector from the center of the α-helix to the center of the hydrophobic patch and the surface normal was also calculated for comparison.

3. RESULTS AND DISCUSSION

3.1. Adsorption Orientation. *PTMC Simulation Results.* In this work, PTMC simulations were performed to study the preliminary adsorption orientations of HFBI on three different surfaces (neutral, negatively charged, and positively charged). The orientation distributions of the electric dipole and the corresponding dominant orientations of HFBI on different surfaces are shown in Figure 2. The results show that the adsorption orientation of HFBI on charged surfaces is dominated by the electric dipole, as indicated by the relatively narrow orientation distributions (red line and blue line in Figure 2). For the neutral surface, several peaks with low probabilities can be observed (black line in Figure 2). All four possible orientations were chosen as the starting points when conducting MD simulations for HFBI adsorption on the CH_3-SAM and OH-SAM.

For HFBI adsorption on the negatively charged surface, the direction of the electric dipole for the preferred orientation (O1) is almost antiparallel to the surface normal. Residues close

dx.doi.org/10.1021/la502595t | *Langmuir* 2014, 30, 11401−11411

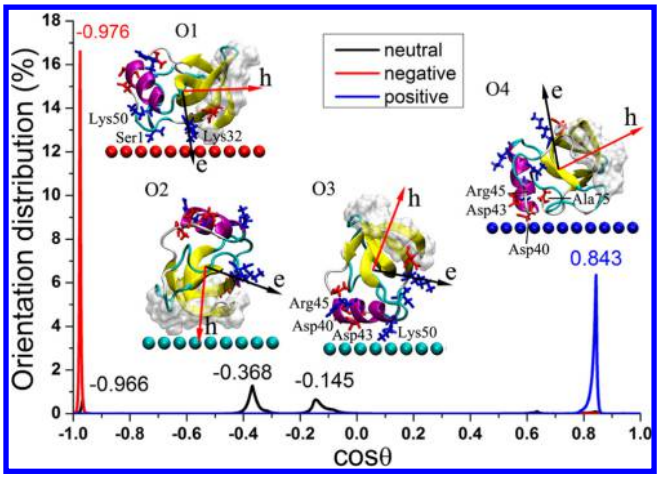

Figure 2. Orientation distributions of the electric dipole and the corresponding dominant orientation of HFBI on different surfaces by PTMC simulations. The red, blue, and black lines represent the orientation distributions of HFBI on negatively charged, positively charged, and neutral surfaces, respectively. O1, O2, O3, and O4 represent the orientations at the peaks of −0.976, −0.368, −0.145, and 0.843, respectively. The surfaces are displayed in VDW mode. Other color policies are the same as those shown in Figure 1.

to the surface are mainly positively charged (Ser1, Lys32, and Lys50). For HFBI adsorption on the positively charged surface, the direction of the electric dipole for the preferred orientation (O4) is almost parallel to the surface normal. Residues near the surface are mainly negatively charged (Asp40, Asp43, and Ala75). For HFBI adsorption on the neutral surface, the directions of the hydrophobic dipole for the two preferred orientations (O2 and O3) are almost perpendicular to the surface. In this case, either the hydrophobic patch (O2) or the α-helix (O3) comes close to the surface.

MD Simulation Results. To investigate the adsorption behaviors of HFBI on different SAM surfaces, 12 different systems were constructed. The four preferred orientations (O1, O2, O3, and O4) obtained from PTMC simulations were chosen as the starting points for MD simulations of HFBI on the CH_3-SAM and OH-SAM. O1 and O4 were chosen as the starting points for the COOH-SAM (7.5 and 15% dissociation degrees) and the NH_2-SAM (7.5 and 15% dissociation degrees), respectively. All of these simulations were conducted for 80 ns. The final snapshots of HFBI adsorbed on different SAM surfaces from MD simulations are shown in Figure 3.

As seen from Figure 3, in most cases, HFBI adsorbs on the hydrophobic CH_3-SAM through its hydrophobic patch and adopts a nearly vertical hydrophobic dipole (Figure 3a) relative to the surface, while, on the hydrophilic OH-SAM, the direction of the hydrophobic dipole is almost parallel to the surface. Previous experiments have showed that the HFBI adsorption onto a hydrophobic surface can reverse the inherent hydrophobicity of the surface, hence making it suitable for immobilization of a secondary protein.[59] For the favorable binding mode of HFBI on the CH_3-SAM (Figure 3a), the hydrophilic region is fully exposed to the solution, leading to a high hydrophilicity of the modified surface, which is consistent with the experimental results.[12] The WCA of the freshly prepared CH_3-SAM was about 92.0°; however, the surfaces were clearly more hydrophilic with WCA between 39 and 56° after HFBI adsorption.[12]

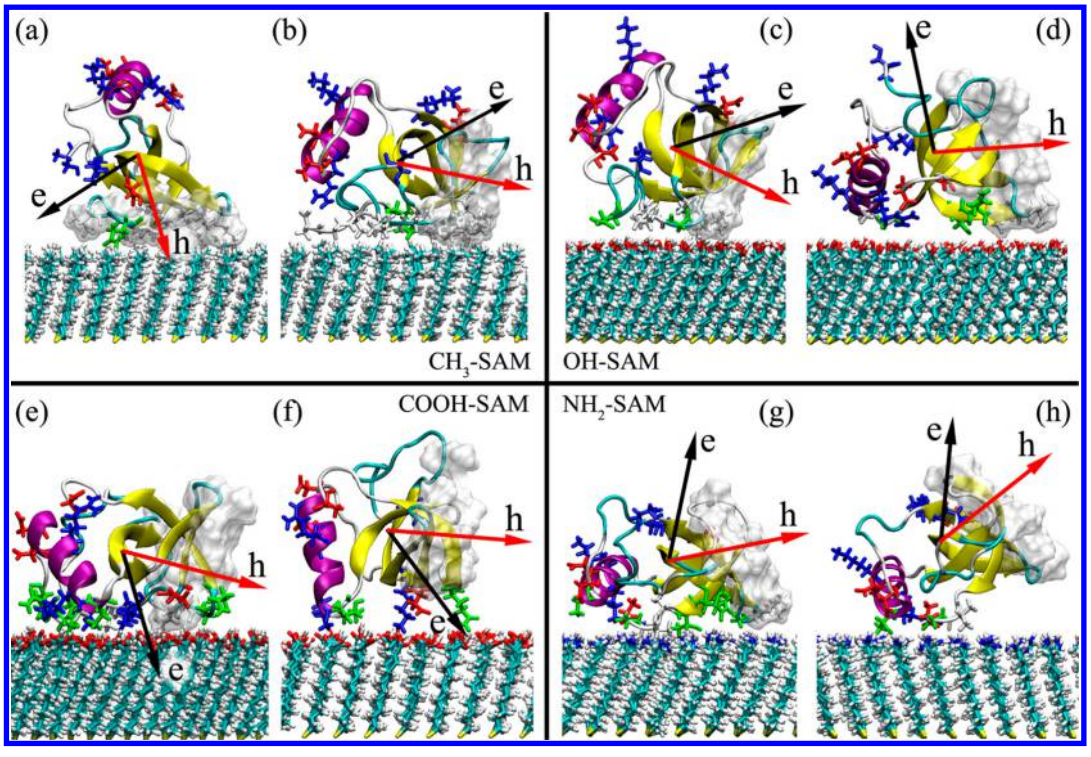

Figure 3. Final snapshots of HFBI adsorbed on different SAM surfaces from MD simulations: (a) from O1, O2, and O3 for HFBI on the CH_3-SAM; (b) from O4 for HFBI on the CH_3-SAM; (c) from O1 for HFBI on the OH-SAM; (d) from O3 and O4 for HFBI on the OH-SAM; (e) for HFBI on the 7.5% dissociated COOH-SAM; (f) for HFBI on the 15% dissociated COOH-SAM; (g) for HFBI on the 7.5% dissociated NH_2-SAM; (h) for HFBI on the 15% dissociated NH_2-SAM. The SAM surfaces are shown in Licorice mode. Residues within 3.5 Å from the surface are shown in Licorice mode and colored by ResType. Water and ions are not shown for clarity. Other color policies are the same as those shown in Figure 1.

dx.doi.org/10.1021/la502595t | *Langmuir* 2014, 30, 11401−11411

For HFBI adsorption on the charged COOH-SAM and NH_2-SAM, the direction of the electric dipole is almost perpendicular to the surface. It is consistent with previous studies that the protein orientation on charged surfaces is dominated by the direction of the electric dipole.[5−7] As seen from Figure 3e−h, the adsorption of HFBI on charged SAMs weakens (as indicated by the decrease of the number of contact residues) as the SCD increases, leading to a larger distance between the SAM surfaces and the hydrophobic patch. Compared with the adsorption on other SAMs, a larger area of the hydrophobic patch is exposed to the solution when HFBI adsorbs on the 15% dissociated NH_2-SAM. In other words, the HFBI adsorption on the positively charged surface leads to an increase of the hydrophobicity of the modified surface. This is consistent with the experimental results that, when HFBI bound to three different kinds of SAM surfaces (cationic, anionic, and hydrophobic), the highest WCA values were obtained on cationic surfaces.[12]

3.2. Orientation Distribution. In order to investigate the orientation distributions of HFBI adsorbed on different SAM surfaces, we use three different angles to characterize it (as defined in section 2.5). The distributions of these orientations were obtained by statistical analysis of the last 20 ns of the MD trajectories for the optimal adsorption modes of HFBI on different SAM surfaces. The results are shown in Figure 4.

Generally, the direction of the helix-patch is most suitable to describe the actual orientation distribution of HFBI on different surfaces because the two regions are very stable during all of the simulations. It is clear that HFBI has the narrowest distribution (Figure 4a) on the CH_3-SAM compared with those on other SAMs, which is suggestive of a steady adsorption. It can self-assemble on the hydrophobic surface to form an ordered monolayer with the hydrophilic region exposed outward, therefore reversing the wettability of the modified surface.[12]

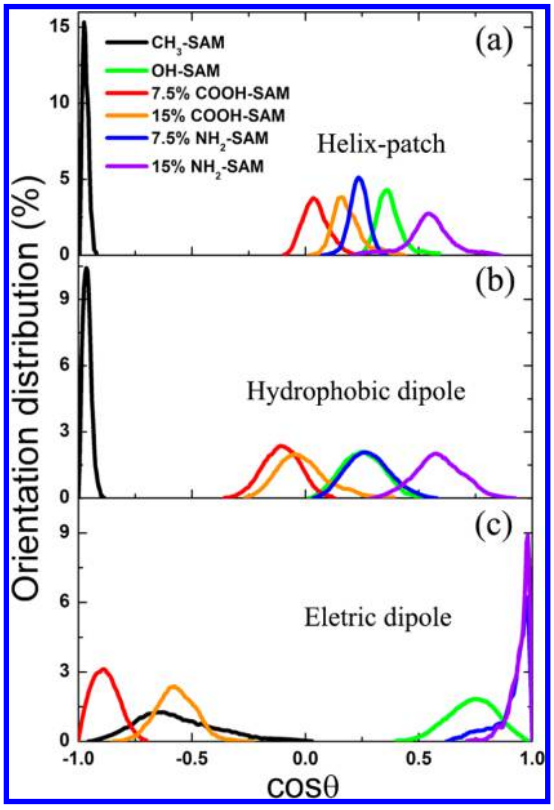

Figure 4. Orientation distributions of HFBI adsorbed on different SAM surfaces by MD simulations for "helix-patch" (a), hydrophobic dipole (b), and electric dipole (c).

The hydrophobic dipole is in the direction almost perpendicular to the surface, as reflected by the value of cos θ (close to −1). Despite the narrowest distribution of the hydrophobic dipole (Figure 4b), it has the widest distribution of the electric dipole (Figure 4c). For HFBI adsorbed on the OH-SAM, it has an almost identical distribution of the hydrophobic dipole compared with that on the 7.5% dissociated NH_2-SAM and adopts an almost horizontal hydrophobic dipole with respect to the surface (Figure 4b).

Although the adsorption energies are lower for HFBI on charged SAMs (especially for COOH-SAM, this will be discussed in more detail in the next section), they actually have wider orientation distributions (Figure 4a). That is to say, the adsorption of HFBI on charged SAMs is not as steady as that on CH_3-SAM. This phenomenon was also found in Soliman et al.'s study[22] that, when the antimicrobial peptide which carries a net charge of +4 e adsorbed on the 50:50 CH_3/COO^- mixed SAMs, the entire peptide moved to the CH_3 surface. They ascribed it to the strong hydrophobic interaction between the hydrophobic side chains of the peptide and CH_3 groups.[22]

The electric dipole is almost perpendicular to the charged surfaces (Figure 4c). For HFBI adsorption on the NH_2-SAM, a relatively wider distribution of the hydrophobic dipole and a narrower distribution of the electric dipole were found, compared with that for the CH_3-SAM. It can be ascribed to the large fluctuation of the position of the N-terminal loop of HFBI when it adsorbs on CH_3-SAM and NH_2-SAM, which will be further discussed in section 3.5. Thus, we can conclude that the movement of these residues is influenced by the nature of the surface. As the SCD increases, the distribution of the electric dipole of HFBI on the NH_2-SAM becomes narrower. Meanwhile, a greater portion of the hydrophobic patch points outward and increases the hydrophobicity of the modified surface, which agrees well with the experimental observations.[12] However, these phenomena were not found for HFBI adsorbed on the COOH-SAM. To further investigate the underlying mechanisms of the different behaviors of HFBI adsorption onto these SAM surfaces, the adsorption energies were calculated and analyzed in detail.

3.3. Interaction Energies. The interaction energies between HFBI and SAM surfaces for all systems are summarized in Table 2. We have also calculated the HFBI−water and SAM−water interaction energies, and the results are listed in Table S1 (Supporting Information). Here, the U_{vdW}, U_{ele}, and U_{tot} (U_{tot} = U_{vdW} + U_{ele}) represent the vdW, electrostatic, and total interaction energies, respectively. It is evident that vdW interactions are much lower and predominant for HFBI adsorption on the CH_3-SAM compared with those on other surfaces. The interactions between the protein and the surface are so strong that a little electrostatic repulsion exists. This indicates that the adsorption of HFBI onto the hydrophobic CH_3-SAM is mainly through hydrophobic interactions. With further observation, we can find that the interaction energy is the lowest for O4 (Figure 3b), although it appears only once, while the other adsorption orientation (Figure 3a) with higher interaction energies occurs three times. This is because the latter (Figure 3a) has a lower free energy than the former (Figure 3b), as revealed in a previous work.[33] They found that the orientation (similar to Figure 3b) with the

dx.doi.org/10.1021/la502595t | Langmuir 2014, 30, 11401−11411

Table 2. Interaction Energies[a] between HFBI and SAM Surfaces

surfaces		U_{vdW} (kJ·mol^{-1})	U_{ele} (kJ·mol^{-1})	U_{tot} (kJ·mol^{-1})
CH_3-SAM	O1/(a)	−166 ± 15	11 ± 2	−155 ± 15
	O2/(a)	−175 ± 14	9 ± 3	−166 ± 13
	O3/(a)	−160 ± 17	10 ± 3	−150 ± 16
	O4/(b)	−198 ± 17	7 ± 3	−191 ± 17
OH-SAM	O1/(c)	−105 ± 16	−14 ± 17	−119 ± 27
	O2			
	O3/(d)	−118 ± 26	−86 ± 43	−204 ± 60
	O4/(d)	−121 ± 27	−130 ± 72	−251 ± 93
COOH-SAM	(e)	−122 ± 33	−571 ± 68	−693 ± 72
	(f)	−47 ± 19	−436 ± 89	−483 ± 81
NH_2-SAM	(g)	−138 ± 20	−189 ± 44	−327 ± 51
	(h)	−69 ± 19	−173 ± 68	−242 ± 76

[a]The energies were averaged over the last 20 ns of MD trajectories, and the errors are the standard deviations.

Table 3. Residues of HFBI in Contact with SAM Surfaces at the End of MD Simulations

Surfaces		Contact residues (< 3.5 Å)*
CH_3-SAM	(a)	Leu12, Leu24, Leu26, Ile27, Leu29, Val59, Ala60, Pro61, Val62, Ala63, Gly64, Gln65, Ala66, Leu67, Leu68
	(b)	Pro9, Pro10, Gly11, Leu12, Phe13, Leu24, Gly25, Leu26, Gln70, Thr71, Val73, Gly74, Ala75
OH-SAM	(c)	Asn4, Pro9, Pro10, Gly11, Leu12, Phe13, Leu24, Leu26, Gln70
	(d)	Thr21, Gln22, Val23, Leu24, Gly25, Arg45, Ala49, Gly52, Gln54
COOH-SAM	(e)	Ser1, Asn2, Lys32, Val33, Ser35, Gln36, Asn37, Lys50, Thr51, Val62, Ala63, Gly64, Gln65
	(f)	Lys32, Lys50, Thr51, Gly52, Gln65
NH_2-SAM	(g)	Gln22, Leu24, Gly25, Thr42, Arg45, Gln70, Thr71, Ala72, Val73, Gly74, Ala75
	(h)	Asp40, Thr42, Arg45, Val73, Gly74, Ala75

*The hydrophobic, positively charged, and negatively charged residues are colored in magenta, blue, and red, respectively.

lowest interaction energy has a higher free energy, while the free energy is much lower for the optimal orientation (similar to Figure 3a).[33]

For HFBI adsorption on the OH-SAM, the energy fluctuation is relatively larger, which has also been found for the adsorption of Aβ peptide on the OH-SAM.[23] The adsorption is mediated through a tightly bound hydration water layer adjacent to the surface (as will be discussed in section 3.7). For the initial orientation O2, the protein cannot even adsorb on the surface. This reveals that the adsorption of HFBI on the hydrophilic OH-SAM is weak and/or reversible, which is consistent with previous simulation results.[23−25] The interaction energy for O4 (Figure 3d) is lower and thus relatively more favorable than the other adsorption orientation (Figure 3c). In this case, the vdW interaction (−121 kJ·mol^{-1}) is close to that of the electrostatic interaction (−130 kJ·mol^{-1}). As a result of the interfacial water layer, the distance between HFBI and the OH-SAM surface is farther than that for the CH_3-SAM, giving rise to lower vdW interaction energies between the protein and the surface.

Although HFBI bears a net charge of zero, its adsorption on charged SAMs is relatively strong and dominated by electrostatic interactions, especially on the COOH-SAM. It has been proved that the distribution of charged residues on the protein surface plays an important role in determining the electrostatic interaction between the protein and the surface.[2,7] For the HFBI adsorption on 7.5% dissociated COOH-SAM, the electrostatic interaction (−571 kJ·mol^{-1}) is nearly 5 times the value of the vdW interaction (−122 kJ·mol^{-1}). In contrast, the electrostatic interaction (−189 kJ·mol^{-1}) is relatively weak and just slightly lower than the vdW interaction (−138 kJ·mol^{-1}) for the 7.5% dissociated NH_2-SAM. For both charged SAMs, as the SCD increases, the vdW interaction decreases significantly, indicating a farther positioning of the protein relative to the surface. However, the decrease of electrostatic interaction is not so obvious after a slight change of the orientations. To further study the key residues dominant in these bindings and to explain the strange behaviors of HFBI on both charged SAMs induced by the increase of SCD, the binding sites were analyzed and the interaction energies between certain residues and the charged SAMs were calculated, as will be discussed in the following section.

3.4. Binding Sites. To explore the key residues responsible for the adsorptions of HFBI on different SAM surfaces, residues of HFBI in contact with the SAM surfaces at the end of the MD simulations were picked out and are summarized in Table 3. The residues containing atoms that are less than 3.5 Å to the surface are considered to be in contact with the surface.

For HFBI on the CH_3-SAM, the adsorbed residues are basically composed of hydrophobic residues, giving rise to favorable desolvation energies. That is to say, the adsorption of HFBI to the hydrophobic CH_3-SAM is mainly through hydrophobic interactions. It is evident that the hydrophobic attraction between HFBI and the CH_3-SAM results in a closer positioning (a larger number of contacted residues) of the protein relative to the surface compared with other SAMs. It is an interesting issue to determine the key residues that are crucial for the adsorption of HFBI on hydrophobic surfaces. Liu et al.[33] proposed that Leu12, Leu24, Leu26, Ile27, Ala66, and Leu68 governed the adsorption of HFBI on different

dx.doi.org/10.1021/la502595t | Langmuir 2014, 30, 11401−11411

hydrophobic surfaces after a comparison with simulation results for HFBI/graphite,[35] HFBI/SWCNT,[36] and HFBI/PDMS.[33] They inferred that the adsorption of HFBI to a hydrophobic surface was mainly contributed by the hydrophobic patch and almost irrespective of the structural feature of the surface.[33] These residues are also found at the interface of HFBI/CH_3-SAM in this work. The adsorbed residues of O1 for the OH-SAM (Figure 3c) are also mainly hydrophobic, which is similar to those of O4 for the CH_3-SAM (Figure 3b). As to O4 for the OH-SAM (Figure 3d), the number of hydrophobic residues remains dominant. This is consistent with the relatively strong vdW interactions (< -100 kJ·mol^{-1}, as shown in Table 2). Similar results have also been found in a previous work; the hydrophobic C-terminal of the Aβ peptide is more likely to be adsorbed on both the CH_3-SAM and OH-SAM.[23]

For HFBI on the COOH-SAM, the adsorbed residues are mainly hydrophilic. With a further investigation of the interaction energies between some of the polar residues of HFBI and the charged SAM surfaces, as summarized in Table S2 (Supporting Information), we can find that the positively charged residues (Ser1, Lys32, and Lys50) play a leading role in the adsorption, which is consistent with PTMC results. For the 7.5 and 15% dissociated COOH-SAM surfaces, these residues account for about 77 and 94% of the total electrostatic interaction energies, respectively. The electrostatic interactions are so strong that there exists a little van der Waals repulsion between the surface and the negatively charged residues. A similar phenomenon was also found for the adsorption of basic fibroblast growth factor on the hydroxyapatite.[46] Correspondingly, the adsorption is mainly induced by the negatively charged residues (Asp40 and Ala75) for HFBI on NH_2-SAM, as can be seen from Table S2 (Supporting Information). For the 7.5%and 15% dissociated NH_2-SAM surfaces, these residues account for about 77 and 93% of the total electrostatic interaction energies, respectively. With a careful comparison, it can be found that the electrostatic interactions between the charged surfaces and the oppositely charged residues accounts for a greater proportion of the total electrostatic interactions with the increase of SCD.

It is evident that the number of contacted residues decreases as the SCD increases for HFBI adsorption on both charged SAMs. Generally, a stronger adsorption is expected with the increase of SCD. However, HFBI has only eight charged residues (including the two terminal residues) and the distribution of these residues is relatively concentrated. The Asp30 and Lys32 are located on one of the β-sheets (residues 27−32) and Asp40, Asp43, Arg45, and Lys50 are on the α-helix (residues 40−50). Furthermore, the C-terminal residue Ala75 is close to Arg45, forming a stable salt bridge. Thus, with the increase of SCD, the electrostatic repulsion between the surfaces and the same charged residues becomes more pronounced. Thus, HFBI has to reorient to make these residues away from the surfaces, which also leads to relatively weaker vdW interactions. Meanwhile, some of the oppositely charged residues try to adopt a closer positioning to compensate for the decrease of the electrostatic attraction, which results in the electrostatic interactions being more concentrated in certain residues.

3.5. Protein Conformation. To explore the structural stability of HFBI adsorbed on different SAM surfaces, the root-mean-square deviation (RMSD) of backbone atoms of HFBI, root-mean-square fluctuation (RMSF) of each residue, R_g, eccentricity, and DSSP (definition of secondary structure of proteins) analysis of HFBI during MD simulations were calculated. The RMSF results are shown in Figure 5. As can

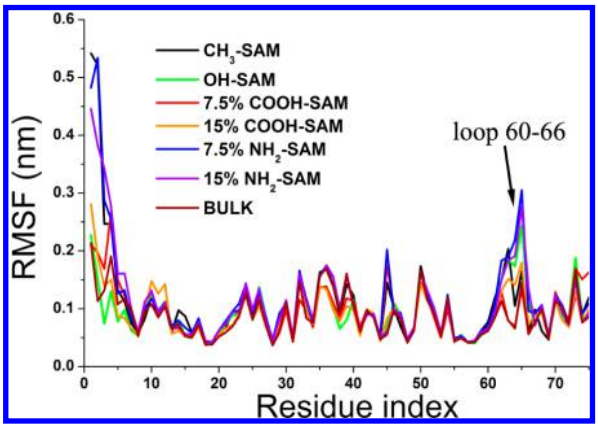

Figure 5. RMSF of atomic positions of each residue of HFBI adsorbed on different SAM surfaces and in bulk solution during MD simulations.

be seen, the RMSF value of the N-terminal of HFBI adsorbed on the OH-SAM and COOH-SAM is relatively low (ca. 2 Å), whereas it is more than 5 Å on the CH_3-SAM and NH_2-SAM. In addition to the N-terminal, the flexible loop (residues 60−66) shows a larger mobility than other parts of HFBI, in particular, for HFBI on the OH-SAM and NH_2-SAM. The same region was found to have a local structural rearrangement in the formation of HFBI tetramer.[29,48] However, the C-terminal was found to be stable during all the MD simulations.

For the COOH-SAM, it bears a certain amount of negative charges, and the N-terminal is positively charged. The electrostatic attraction leads to the N-terminal residue (Ser1) approaching the surface; thus, its movement is extremely restricted. However, for the CH_3-SAM, there is no such attraction, so this region has greater freedom. In contrast, for the NH_2-SAM, there exists a certain amount of electrostatic repulsion, which makes the N-terminal region move away from the surface. It in turn limits its mobility to a certain extent. This explains why HFBI has the narrowest distribution of the hydrophobic dipole and the widest distribution of the electric dipole on the CH_3-SAM. The same explanation is also applicable for HFBI on the NH_2-SAM. Furthermore, due to the formation of a stable salt bridge between the carboxyl group of the C-terminal residue (Ala75) and the guanidine of Arg45, the mobility of the C-terminal is greatly restricted.

The DSSP analysis for HFBI on different SAM surfaces during MD simulations is shown in Figure S1 (Supporting Information). Evidently, there are relatively large fluctuations of the N-terminal loop of HFBI for almost all surfaces (except for the COOH-SAM). For the OH-SAM and NH_2-SAM, there are also larger fluctuations in the flexible loop 60−66. However, the main secondary structures, such as the α-helix and β-sheet, are preserved in the course of adsorption, which may be attributed to the four strong disulfide bonds.[29] Additionally, an interesting structural transformation of the region near the N-terminal can be found for HFBI on the 7.5% dissociated NH_2-SAM. Some turn structure formed during the simulation, while this region mainly switched between the turn structure and bend structure for HFBI adsorbed on other surfaces.

To quantitatively describe the conformation changes of HFBI, the averaged properties of HFBI in bulk solution and adsorbed on SAM surfaces together with those of the crystal

dx.doi.org/10.1021/la502595t | Langmuir 2014, 30, 11401−11411

Table 4. Averaged Properties of HFBI in Bulk Solution and Adsorbed on SAM Surfaces

		R_g (Å)	eccentricity	RMSD (Å)	electric dipole moment (D)	hydrophobic dipole moment (nm)
crystal		10.6	0.15		104	16.1
bulk		10.9	0.17	1.8 ± 0.2	106 ± 18	12.6 ± 1.0
CH_3-SAM	(a)	11.0	0.18	2.3 ± 0.5	65 ± 20	14.1 ± 1.1
	(b)	11.0	0.16	2.2 ± 0.1	111 ± 17	15.2 ± 0.8
OH-SAM	(c)	11.0	0.18	2.4 ± 0.1	102 ± 18	12.8 ± 0.9
	(d)	10.8	0.16	1.2 ± 0.1	128 ± 17	12.6 ± 0.8
COOH-SAM	(e)	10.8	0.16	1.0 ± 0.1	130 ± 14	12.8 ± 0.9
	(f)	10.8	0.16	1.2 ± 0.1	127 ± 12	13.6 ± 0.8
NH_2-SAM	(g)	11.0	0.18	2.6 ± 0.5	86 ± 24	13.9 ± 1.1
	(h)	10.9	0.17	2.3 ± 0.3	132 ± 15	13.5 ± 1.2

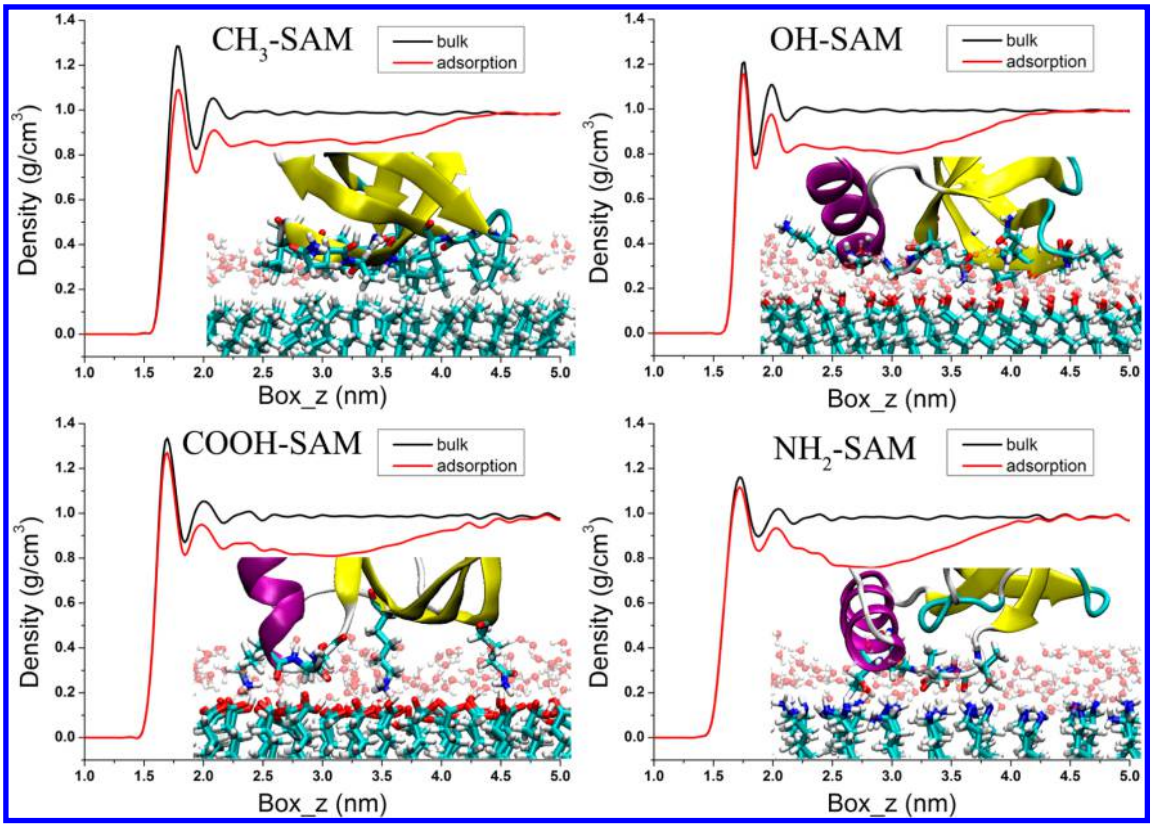

Figure 6. Density profiles of water molecules along the surface normal for four different SAMs in solution before and after HFBI adsorption. The four insets show the corresponding adsorption configurations of protein near SAM surfaces. The protein is represented in NewCartoon mode and the SAMs in Licorice mode. Water molecules that are within 5 Å of the SAM surfaces are shown in CPK mode with a transparent representation. Residues that are within 3.5 Å from surfaces are shown in the Licorice mode.

structure were calculated and the results are summarized in Table 4. It can be found that the RMSD of HFBI on the OH-SAM and COOH-SAM (ca. 1.0−1.2 Å) are generally lower than those in the bulk solution (ca. 1.8 Å), except for the unfavorable adsorption (Figure 2c) of HFBI on OH-SAM (ca. 2.4 Å), indicating that the adsorption of HFBI on these surfaces makes its structure more stable. With several repeated simulations, it can be found that the unfavorable adsorption modes always lead to a larger mobility of the N-terminal loop. In contrast, RMSD values of HFBI on the CH_3-SAM and NH_2-SAM go up to ca. 2.2−2.6 Å, indicating a larger structural deformation. These structural changes mainly come from the N-terminal loop of HFBI, as discussed above.

The overall size of HFBI was monitored by calculating the radius of gyration (R_g). As shown in Table 4, the average value is about 10.8−11.0 Å and no significant changes of the size of HFBI were observed for all SAM surfaces. The value of R_g is close to that calculated for HFBI adsorbed on the PDMS surface (ca. 10.8−11.4 Å)[33] but a little lower than that calculated from the crystal structure of HFBI (14.0 Å).[32,49] This may be because the latter was averaged over all four monomers presented in the crystal structure, while here only monomer A was taken into consideration. In the tetramer, the structures of monomers B and D have a more extended conformation in loop 60−66 than those of monomers A and C.[29,33] Moreover, the overall shape of HFBI is characterized by the eccentricity, which is defined as $1 - I_{ave}/I_{max}$, where I_{max} is the maximal principal moment of inertia and I_{ave} is the average of three principal moments of inertia.[6,7] The eccentricity is zero for a perfect sphere and close to 1 for a flat or needlelike ellipsoid.[33] The average eccentricity for all the systems is about 0.16−0.18, indicating that the shape of HFBI after absorption is close to a

dx.doi.org/10.1021/la502595t | Langmuir 2014, 30, 11401−11411

sphere and there is no significant change of tertiary structure during MD simulations.

3.6. Role of Electric Dipole and Hydrophobic Dipole. The averaged values of the hydrophobic dipole moment and electric dipole moment during MD simulations are also shown in Table 4. It can be found that the value of the electric dipole moment in the bulk solution (106 D) is very close to that of the crystal structure (104 D). For the optimal adsorption mode on the CH_3-SAM surface, its value (65 D) reduces to a great extent. However, for charged surfaces, this value increases significantly, except for the 7.5% dissociated NH_2-SAM (86 D). This is consistent with the general law that the adsorption of a protein to a charged surface often leads to an increase of electric dipole moment.[6] Seeing such a big fluctuation of the electric dipole moment, we may be curious why this happens. As there are only eight charged residues for HFBI, a large fluctuation of the position of any charged residue can lead to a substantial variation of the electric dipole moment.

We can find from Table 4 that the value of the hydrophobic dipole moment of the crystal structure of HFBI is 16.1 nm, which is larger than that on any other surface. Compared with the values on other surfaces, the values for HFBI on the CH_3-SAM (14.1 and 15.2 nm) are much closer to that of the crystal structure, followed by the NH_2-SAM (13.5 and 13.9 nm). For HFBI in the bulk solution and on the hydrophilic OH-SAM, the values are generally low (12.6−12.8 nm). Since the protein used in these simulations is one monomer extracted from the tetramer crystal structure[29] and the four HFBI molecules in this tetramer gather together through the hydrophobic patch, this means that the HFBI structure in the tetramer is almost equivalent to that adsorbed on a hydrophobic surface. Furthermore, from the values of the hydrophobic dipole moment of HFBI adsorbed on these SAM surfaces, we can conclude that the effect of the hydrophobic dipole on the adsorption of proteins onto hydrophobic surfaces is similar to that of the electric dipole on the adsorption of proteins onto charged surfaces. That is, the adsorption of a protein on a hydrophobic surface leads to the direction of the hydrophobic dipole being almost perpendicular to the surface and an increase of its magnitude.

3.7. Role of Interfacial Water. The water behaviors near SAM surfaces at the molecular level have direct implications on a variety of processes, such as binding of proteins to surfaces and biological self-assembly in interfacial environments.[60] To further study the impact of water layers near SAM surfaces on the binding of HFBI to these surfaces, the density profiles of water molecules along the surface normal for four different SAMs in solution before and after HFBI adsorption were calculated. The data with protein adsorption were averaged over the last 20 ns of MD trajectories for the optimal adsorption modes of HFBI on these SAMs. The corresponding adsorption configurations near the SAM surfaces are also shown in Figure 6.

It is obvious that there are two water layers formed near all four SAM surfaces. Compared with the OH-SAM and NH_2-SAM, the densities of water molecules near surfaces are relatively higher for the CH_3-SAM and COOH-SAM. After the protein adsorption, the density of both water layers near the CH_3-SAM decreases significantly. For the OH-SAM, the density of the first water layer is almost unchanged and only that of the second water layer has an obvious decrease. As for the COOH-SAM and NH_2-SAM, the local density of the first water layer slightly reduces because of the strong electrostatic attraction between HFBI and surfaces, leading to a closer positioning of some of the oppositely charged residues to surfaces.

From the insets in Figure 6, we can find that the adsorption of HFBI on the CH_3-SAM leads to the removal of water molecules near the hydrophobic surface and several residues pass through water layers to form a direct contact with the surface. As analyzed above, the residues near the surface are mainly hydrophobic. That is to say, the adsorption of HFBI on the hydrophobic surface is mainly through hydrophobic interactions via the desolvation of the surface and the protein. For the OH-SAM, it is evident that the protein adsorption is mediated through a hydration water layer near the surface. Previous simulations have demonstrated that there is a strong interaction between the interfacial water and the OH-SAM, due to the formation of a large number of hydrogen bonds at the interface.[23−25] Therefore, further approach of HFBI to the surface is hindered, leading to a relatively weak adsorption. For charged SAMs, the adsorption leads to some of the oppositely charged residues (or groups) approaching the surfaces, forming stable salt bridges at the interfaces. Although these surfaces are also highly hydrated,[24] the strong attractive electrostatic interactions can sufficiently compensate the energy penalty for breaking the network of hydrogen bonds at interfaces, leading to HFBI adsorption.

4. CONCLUSIONS

In this work, the adsorptions of HFBI on four different SAM surfaces (i.e., CH_3-SAM, OH-SAM, COOH-SAM, and NH_2-SAM) were investigated by a combined PTMC and MD simulation approach. Simulation results show that HFBI adsorbs on the hydrophobic CH_3-SAM through its hydrophobic patch and adopts a nearly vertical hydrophobic dipole relative to the surface, while the hydrophobic dipole of HFBI is almost parallel to the hydrophilic OH-SAM surface. Correspondingly, HFBI adopts a nearly vertical electric dipole relative to the charged SAM surfaces. Relative to other surfaces, HFBI actually has the narrowest orientation distribution on the CH_3-SAM. It can self-assemble and form an ordered monolayer with the hydrophilic region exposed to the solution, reversing the wettability of the surface. Interestingly, the adsorption strength of HFBI on charged SAMs weakens with the increase of SCD. Compared with those on other SAMs, a greater portion of the hydrophobic patch is exposed to the solution when it adsorbs on the NH_2-SAM. In other words, HFBI adsorption on the positively charged surface leads to an increase of the hydrophobicity of the surface, which is consistent with the experimental results.

The binding of HFBI to the CH_3-SAM is mainly through hydrophobic interactions via the desolvation of the surface and the protein. The protein adsorption is mediated through a hydration water layer near the surface for the OH-SAM. For charged SAMs, the adsorption is mainly induced by electrostatic interactions between the charged surfaces and the oppositely charged residues. There are larger fluctuations of the positions of the N-terminal loop for HFBI adsorbed on the CH_3-SAM and NH_2-SAM than those on the OH-SAM and COOH-SAM. However, the main secondary structures, such as the α-helix and β-sheet, are preserved in the course of adsorption due to four disulfide bonds.

The effect of a hydrophobic dipole on protein adsorption onto hydrophobic surfaces is similar to that of an electric dipole on protein adsorption onto charged surfaces. That is, the

adsorption of a protein on a hydrophobic surface leads to the direction of the hydrophobic dipole being almost perpendicular to the surface. The hydrophobic dipole could be generally applied to predict the probable orientations of other proteins adsorbed on hydrophobic surfaces.

■ ASSOCIATED CONTENT

Supporting Information

Details on the interaction energies of HFBI−water and SAM−water (Table S1), interaction energies between polar residues and the charged surfaces (Table S2), and DSSP analysis along MD simulations (Figure S1). This material is available free of charge via the Internet at http://pubs.acs.org.

■ AUTHOR INFORMATION

Corresponding Author

*E-mail: jianzhou@scut.edu.cn.

Notes

The authors declare no competing financial interest.

■ ACKNOWLEDGMENTS

This work is supported by the National Key Basic Research Program of China (No. 2013CB733500), National Natural Science Foundation of China (Nos. 21376089, 91334202), the Fundamental Research Funds for the Central Universities (SCUT-2013ZM0073), and State Key Laboratory of Materials-Oriented Chemical Engineering (KL12-05). The computational resources for this project are provided by SCUTGrid at South China University of Technology.

■ REFERENCES

(1) Abramyan, T.; Collier, G.; Kucukkal, T. G.; Li, X.; Snyder, J. A.; Thyparambil, A. A.; Vellore, N. A.; Wei, Y.; Yancey, J. A.; Stuart, S. J.; Latour, R. A. Understanding Protein-Surface Interactions at the Atomistic Level through the Synergistic Development of Experimental and Molecular Simulation Methods. *Proteins at Interfaces III State of the Art*; American Chemical Society: Washington, DC, 2012; Vol. *1120*, pp 197−228.

(2) Ravichandran, S.; Madura, J. D.; Talbot, J. A Brownian Dynamics Study of the Initial Stages of Hen Egg-White Lysozyme Adsorption at a Solid Interface. *J. Phys. Chem. B* **2001**, *105*, 3610−3613.

(3) Chen, S. F.; Liu, L. Y.; Zhou, J.; Jiang, S. Y. Controlling antibody orientation on charged self-assembled monolayers. *Langmuir* **2003**, *19*, 2859−2864.

(4) Zhou, J.; Chen, S. F.; Jiang, S. Y. Orientation of adsorbed antibodies on charged surfaces by computer simulation based on a united-residue model. *Langmuir* **2003**, *19*, 3472−3478.

(5) Xie, Y.; Zhou, J.; Jiang, S. Y. Parallel tempering Monte Carlo simulations of lysozyme orientation on charged surfaces. *J. Chem. Phys.* **2010**, *132*, 065101.

(6) Zhou, J.; Zheng, J.; Jiang, S. Y. Molecular simulation studies of the orientation and conformation of cytochrome c adsorbed on self-assembled monolayers. *J. Phys. Chem. B* **2004**, *108*, 17418−17424.

(7) Liu, J.; Liao, C. Y.; Zhou, J. Multiscale Simulations of Protein G B1 Adsorbed on Charged Self-Assembled Monolayers. *Langmuir* **2013**, *29*, 11366−11374.

(8) Zhao, D. H.; Peng, C. W.; Liao, C. Y.; Zhou, J. Computer simulation of bioenergy-oriented enzyme immobilization. *CIESC J.* **2014**, *65*, 1828−1834.

(9) Schlapak, R.; Armitage, D.; Saucedo-Zeni, N.; Chrzanowski, W.; Hohage, M.; Caruana, D.; Howorka, S. Selective protein and DNA adsorption on PLL-PEG films modulated by ionic strength. *Soft Matter* **2009**, *5*, 613−621.

(10) Pasche, S.; Vörös, J.; Griesser, H. J.; Spencer, N. D.; Textor, M. Effects of Ionic Strength and Surface Charge on Protein Adsorption at PEGylated Surfaces. *J. Phys. Chem. B* **2005**, *109*, 17545−17552.

(11) Borges, J.; Campiña, J. M.; Silva, A. F. Probing the Contribution of Different Intermolecular Forces to the Adsorption of Spheroproteins onto Hydrophilic Surfaces. *J. Phys. Chem. B* **2013**, *117*, 16565−16576.

(12) Grunér, M. S.; Szilvay, G. R.; Berglin, M.; Lienemann, M.; Laaksonen, P.; Linder, M. B. Self-assembly of Class II Hydrophobins on Polar Surfaces. *Langmuir* **2012**, *28*, 4293−4300.

(13) Yu, G. B.; Liu, J.; Zhou, J. Mesoscopic Coarse-Grained Simulations of Lysozyme Adsorption. *J. Phys. Chem. B* **2014**, *118*, 4451−4460.

(14) Eisenberg, D.; Weiss, R. M.; Terwilliger, T. C.; Wilcox, W. Hydrophobic moments and protein structure. *Faraday Symp. Chem. Soc.* **1982**, *17*, 109−120.

(15) Eisenberg, D.; Schwarz, E.; Komaromy, M.; Wall, R. Analysis of membrane and surface protein sequences with the hydrophobic moment plot. *J. Mol. Biol.* **1984**, *179*, 125−142.

(16) Harris, F.; Wallace, J.; Phoenix, D. A. Use of hydrophobic moment plot methodology to aid the identification of oblique orientated alpha-helices. *Mol. Membr. Biol.* **2000**, *17*, 201−207.

(17) Phoenix, D. A.; Harris, F. The hydrophobic moment and its use in the classification of amphiphilic structures (Review). *Mol. Membr. Biol.* **2002**, *19*, 1−10.

(18) Wallace, J.; Daman, O. A.; Harris, F.; Phoenix, D. A. Investigation of hydrophobic moment and hydrophobicity properties for transmembrane alpha-helices. *Theor. Biol. Med. Modell.* **2004**, *1*, 5.

(19) Eisenberg, D.; Weiss, R. M.; Terwilliger, T. C. The hydrophobic moment detects periodicity in protein hydrophobicity. *Proc. Natl. Acad. Sci. U. S. A.* **1984**, *81*, 140−144.

(20) Silverman, B. D. Hydrophobic moments of tertiary protein structures. *Proteins: Struct., Funct., Genet.* **2003**, *53*, 880−888.

(21) Horinek, D.; Serr, A.; Geisler, M.; Pirzer, T.; Slotta, U.; Lud, S.; Garrido, J.; Scheibel, T.; Hugel, T.; Netz, R. Peptide adsorption on a hydrophobic surface results from an interplay of solvation, surface, and intrapeptide forces. *Proc. Natl. Acad. Sci. U. S. A.* **2008**, *105*, 2842−2847.

(22) Soliman, W.; Bhattacharjee, S.; Kaur, K. Adsorption of an antimicrobial peptide on self-assembled monolayers by molecular dynamics simulation. *J. Phys. Chem. B* **2010**, *114*, 11292−11302.

(23) Wang, Q.; Zhao, C.; Zhao, J.; Wang, J.; Yang, J.-C.; Yu, X.; Zheng, J. Comparative Molecular Dynamics Study of Aβ Adsorption on the Self-Assembled Monolayers. *Langmuir* **2009**, *26*, 3308−3316.

(24) Wang, Q.; Zhao, J.; Yu, X.; Zhao, C.; Li, L.; Zheng, J. Alzheimer Aβ_{1-42} Monomer Adsorbed on the Self-Assembled Monolayers. *Langmuir* **2010**, *26*, 12722−12732.

(25) Xie, Y.; Liu, M. F.; Zhou, J. Molecular dynamics simulations of peptide adsorption on self-assembled monolayers. *Appl. Surf. Sci.* **2012**, *258*, 8153−8159.

(26) Chen, S.; Zheng, J.; Li, L.; Jiang, S. Strong Resistance of Phosphorylcholine Self-Assembled Monolayers to Protein Adsorption: Insights into Nonfouling Properties of Zwitterionic Materials. *J. Am. Chem. Soc.* **2005**, *127*, 14473−14478.

(27) Linder, M. B. Hydrophobins: Proteins that self assemble at interfaces. *Curr. Opin. Colloid Interface Sci.* **2009**, *14*, 356−363.

(28) Linder, M. B.; Szilvay, G. R.; Nakari-Setälä, T.; Penttilä, M. E. Hydrophobins: the protein-amphiphiles of filamentous fungi. *FEMS Microbiol. Rev.* **2005**, *29*, 877−896.

(29) Hakanpää, J.; Szilvay, G. R.; Kaljunen, H.; Maksimainen, M.; Linder, M. B.; Rouvinen, J. Two crystal structures of Trichoderma reesei hydrophobin HFBI—The structure of a protein amphiphile with and without detergent interaction. *Protein Sci.* **2006**, *15*, 2129−2140.

(30) Hektor, H. J.; Scholtmeijer, K. Hydrophobins: proteins with potential. *Curr. Opin. Biotechnol.* **2005**, *16*, 434−439.

(31) Khalesi, M.; Deckers, S. M.; Gebruers, K.; Vissers, L.; Verachtert, H.; Derdelinckx, G. Hydrophobins: Exceptional proteins

for many applications in brewery environment and other bio-industries. *Cerevisia* **2012**, *37*, 3−9.
(32) Krivosheeva, O.; Dėdinaitė, A.; Linder, M. B.; Tilton, R. D.; Claesson, P. M. Kinetic and Equilibrium Aspects of Adsorption and Desorption of Class II Hydrophobins HFBI and HFBII at Silicon Oxynitride/Water and Air/Water Interfaces. *Langmuir* **2013**, *29*, 2683−2691.
(33) Liu, Y. Z.; Wu, M.; Feng, X. Z.; Shao, X. G.; Cai, W. S. Adsorption Behavior of Hydrophobin Proteins on Polydimethylsiloxane Substrates. *J. Phys. Chem. B* **2012**, *116*, 12227−12234.
(34) Moldovan, C.; Thompson, D. Molecular dynamics of the "hydrophobic patch" that immobilizes hydrophobin protein HFBII on silicon. *J. Mol. Model.* **2011**, *17*, 2227−2235.
(35) Mereghetti, P.; Wade, R. Diffusion of hydrophobin proteins in solution and interactions with a graphite surface. *BMC Biophys.* **2011**, *4*, 1−11.
(36) Liu, Y. Z.; Cai, W. S.; Shao, X. G. Molecular Dynamics Simulation of Hydrophobin Proteins on the Surface of Single-walled Carbon Nanotubes. *Chem. J. Chin. Univ.* **2012**, *33*, 2013−2018.
(37) O'Mahony, S.; O'Dwyer, C.; Nijhuis, C. A.; Greer, J. C.; Quinn, A. J.; Thompson, D. Nanoscale Dynamics and Protein Adhesivity of Alkylamine Self-Assembled Monolayers on Graphene. *Langmuir* **2013**, *29*, 7271−7282.
(38) Cheung, D. L. Molecular Simulation of Hydrophobin Adsorption at an Oil−Water Interface. *Langmuir* **2012**, *28*, 8730−8736.
(39) Euston, S. R. Molecular simulation of adsorption of hydrophobin HFBI to the air−water, DPPC−water and decane−water interfaces. *Food Hydrocolloids* **2013**, 1−9.
(40) Wei, T.; Carignano, M. A.; Szleifer, I. Lysozyme Adsorption on Polyethylene Surfaces: Why Are Long Simulations Needed? *Langmuir* **2011**, *27*, 12074−12081.
(41) Yu, X.; Wang, Q.; Lin, Y.; Zhao, J.; Zhao, C.; Zheng, J. Structure, Orientation, and Surface Interaction of Alzheimer Amyloid-β Peptides on the Graphite. *Langmuir* **2012**, *28*, 6595−6605.
(42) Wei, T.; Carignano, M. A.; Szleifer, I. Molecular Dynamics Simulation of Lysozyme Adsorption/Desorption on Hydrophobic Surfaces. *J. Phys. Chem. B* **2012**, *116*, 10189−10194.
(43) Yang, C.; Peng, C. W.; Zhao, D. H.; Liao, C. Y.; Zhou, J.; Lu, X. H. Molecular simulations of myoglobin adsorbed on rutile (110) and (001) surfaces. *Fluid Phase Equilib.* **2014**, *362*, 349−354.
(44) Yang, C.; Peng, C. W.; Liao, C. Y.; Zhou, J. Computer Simulations of Fibronectin Adsorption on Graphene Modified Titanium Dioxide Surfaces. *Acta Chim. Sin.* **2014**, *72*, 401−406.
(45) Liao, C. Y.; Xie, Y.; Zhou, J. Computer simulations of fibronectin adsorption on hydroxyapatite surfaces. *RSC Adv.* **2014**, *4*, 15759−15769.
(46) Liao, C.; Zhou, J. Replica-Exchange Molecular Dynamics Simulation of Basic Fibroblast Growth Factor Adsorption on Hydroxyapatite. *J. Phys. Chem. B* **2014**, *118*, 5843−5852.
(47) Kyte, J.; Doolittle, R. F. A simple method for displaying the hydropathic character of a protein. *J. Mol. Biol.* **1982**, *157*, 105−132.
(48) Szilvay, G. R.; Nakari-Setälä, T.; Linder, M. B. Behavior of Trichoderma reesei Hydrophobins in Solution: Interactions, Dynamics, and Multimer Formation. *Biochemistry* **2006**, *45*, 8590−8598.
(49) Kisko, K.; Szilvay, G. R.; Vainio, U.; Linder, M. B.; Serimaa, R. Interactions of Hydrophobin Proteins in Solution Studied by Small-Angle X-Ray Scattering. *Biophys. J.* **2008**, *94*, 198−206.
(50) Szilvay, G. R.; Kisko, K.; Serimaa, R.; Linder, M. B. The relation between solution association and surface activity of the hydrophobin HFBI from Trichoderma reesei. *FEBS Lett.* **2007**, *581*, 2721−2726.
(51) Guex, N.; Peitsch, M. C. SWISS-MODEL and the Swiss-Pdb Viewer: an environment for comparative protein modeling. *Electrophoresis* **1997**, *18*, 2714−2723.
(52) Hess, B.; Kutzner, C.; van der Spoel, D.; Lindahl, E. GROMACS 4: Algorithms for Highly Efficient, Load-Balanced, and Scalable Molecular Simulation. *J. Chem. Theory Comput.* **2008**, *4*, 435−447.
(53) MacKerell, A. D.; Bashford, D.; Bellott; Dunbrack, R. L.; Evanseck, J. D.; Field, M. J.; Fischer, S.; Gao, J.; Guo, H.; Ha, S.; Joseph-McCarthy, D.; Kuchnir, L.; Kuczera, K.; Lau, F. T. K.; Mattos, C.; Michnick, S.; Ngo, T.; Nguyen, D. T.; Prodhom, B.; Reiher, W. E.; Roux, B.; Schlenkrich, M.; Smith, J. C.; Stote, R.; Straub, J.; Watanabe, M.; Wiórkiewicz-Kuczera, J.; Yin, D.; Karplus, M. All-Atom Empirical Potential for Molecular Modeling and Dynamics Studies of Proteins. *J. Phys. Chem. B* **1998**, *102*, 3586−3616.
(54) Jorgensen, W. L.; Chandrasekhar, J.; Madura, J. D.; Impey, R. W.; Klein, M. L. Comparison of simple potential functions for simulating liquid water. *J. Chem. Phys.* **1983**, *79*, 926.
(55) Hoover, W. G. Canonical dynamics: equilibrium phase-space distributions. *Phys. Rev. A* **1985**, *31*, 1695.
(56) Hess, B.; Bekker, H.; Berendsen, H. J. C.; Fraaije, J. G. E. M. LINCS: a linear constraint solver for molecular simulations. *J. Comput. Chem.* **1997**, *18*, 1463−1472.
(57) Yeh, I. C.; Berkowitz, M. L. Ewald summation for systems with slab geometry. *J. Chem. Phys.* **1999**, *111*, 3155−3162.
(58) Humphrey, W.; Dalke, A.; Schulten, K. VMD: visual molecular dynamics. *J. Mol. Graphics* **1996**, *14*, 33−38.
(59) Wang, Z. F.; Lienemann, M.; Qiao, M. Q.; Linder, M. B. Mechanisms of Protein Adhesion on Surface Films of Hydrophobin. *Langmuir* **2010**, *26*, 8491−8496.
(60) Xu, Z.; Song, K.; Yuan, S. L.; Liu, C. B. Microscopic wetting of self-assembled monolayers with different surfaces: A combined molecular dynamics and quantum mechanics study. *Langmuir* **2011**, *27*, 8611−8620.

Supporting Information for

Adsorption of Hydrophobin on Different Self-assembled Monolayers: the Role of the Hydrophobic Dipole and the Electric Dipole

*Chunwang Peng, Jie Liu, Daohui Zhao, Jian Zhou**

School of Chemistry and Chemical Engineering, Guangdong Provincial Key Lab for Green Chemical Product Technology, South China University of Technology, Guangzhou, Guangdong, 510640, P. R. Chin

Table S1. Interaction energies between HFBI, SAM surfaces and water molecules.

Surfaces		HFBI-water (kJ·mol^{-1})		SAM-water (kJ·mol^{-1})	
		U_{ele}	U_{vdW}	U_{ele}	U_{vdW}
CH_3-SAM	O1/(a)	−4585±204	−480±57	55±10	−697±30
	O2/(a)	−4639±206	−455±63	58±10	−687±30
	O3/(a)	−4568±215	−438±59	56±10	−696±31
	O4/(b)	−4466±211	−473±66	59±10	−691±30
OH-SAM	O1/(c)	−4808±184	−561±64	−6854±193	325±87
	O2	–	–	–	–
	O3/(d)	−4766±236	−498±65	−6756±195	331±83
	O4/(d)	−4613±209	−531±63	−6700±198	332±84
COOH-SAM	(e)	−4178±203	−525±62	−6158±322	53±84
	(f)	−4193±178	−566±65	−6381±341	14±85
NH_2-SAM	(g)	−4499±200	−514±62	−6136±282	−306±88
	(h)	−4474±270	−581±63	−5461±345	−224±84

From Table S1, we can find that: (1) the stronger interactions between HFBI and SAM, the weaker interactions between HFBI and water; (2) the SAM-water interactions are basically not influenced by different adsorption orientations; (3) there exists a weak electrostatic repulsion between CH_3-SAM and water while the vdW interactions between them are the strongest; (4) there exists a strong vdW repulsion between OH-SAM and water while the electrostatic interactions between them are the strongest.

Table S2. Interaction energies between polar residues of HFBI and charged SAM surfaces

Surfaces		Residue	U_{vdw} (kJ·mol^{-1})	U_{ele} (kJ·mol^{-1})	U_{tot} (kJ·mol^{-1})
COOH-SAM	(e)	**Ser1(+)**	6±10	**−217±37**	−211±32
		Lys32	−2±9	**−160±49**	−162±45
		Lys50	−6±6	**−65±41**	−71±40
		Asn2	−13±6	−45±18	−58±16
		Asn37	−10±5	−21±19	−31±19
		Gln36	−14±4	−9±12	−23±13
	(f)	**Lys50**	−1±11	**−219±34**	−220±28
		Lys32	3±10	**−190±40**	−187±34
		Thr51	−17±4	−8±14	−25±14
		Gln65	−11±6	−4±24	−15±25
NH_2-SAM	(g)	**Ala75(−)**	0±7	**−146±21**	−146±18
		Thr71	−12±5	−13±14	−25±11
		Gln22	−10±5	−8±10	−18±13
	(h)	**Ala75(−)**	−1±6	**−108±54**	−109±52
		Asp40	−3±5	**−53±50**	−56±49
		Thr42	−14±5	−8±8	−22±9

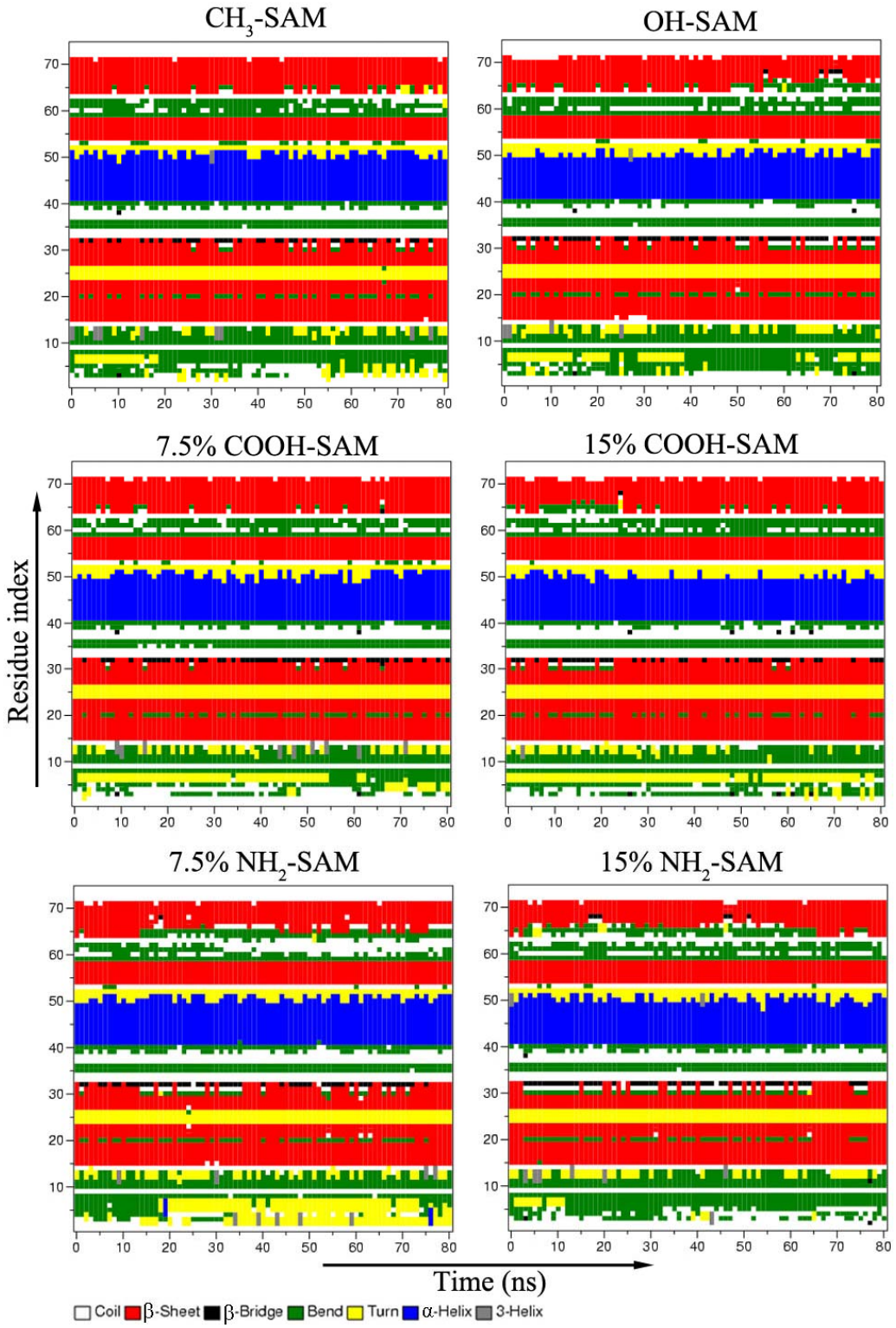

Figure S1. DSSP secondary structure assignments during MD simulations for HFBI on different SAM surfaces.